Bull Volcanol (1989) 51:299-310

Bulletin of Volcanology

Anisotropy of magnetic susceptibility in welded tuffs: application to a welded-tuff dyke in the Tertiary Trans-Pecos Texas volcanic province, USA

John A Wolff, Brooks B Ellwood, and Scott D Sachs

Department of Geology, University of Texas at Arlington, Arlington, TX 76019, USA

Abstract. Consideration of published anisotropy of magnetic susceptibility (AMS) studies on welded ignimbrites suggests that AMS fabrics are controlled by groundmass microlites distributed within the existing tuff fabric, the sum result of directional fabrics imposed by primary flow lineation, welding, and (if relevant) rheomorphism. AMS is a more sensitive indicator of fabric elements within welded tuffs than conventional methods, and usually yields primary flow azimuth estimates. Detailed study of a single densely welded tuff sample demonstrates that the overall AMS fabric is insensitive to the relative abundances of fiamme, matrix and lithics within individual drilled cores. AMS determinations on a welded-tuff dyke occurring in a choked vent in the Trans-Pecos Texas volcanic field reveals a consistent fabric with a prolate element imbricated with respect to one wall of the dyke, while total magnetic susceptibility and density exhibit axially symmetric variations across the dyke width. The dyke is interpreted to have formed as a result of agglutination of the erupting mixture on a portion of the conduit wall as it failed and slid into the conduit, followed by residual squeezing between the failed block and in situ wallrock. Irrespective of the precise mechanism, widespread occurrence of both welded-tuff dykes and point-welded, aggregate pumices in pyroclastic deposits may imply that lining of conduit walls by agglutionation during explosive volcanic eruptions is a common process.

Introduction

Rock magnetic methods have a potentially wide application in volcanology, as indicators of the thermal and mechanical histories of volcanic rocks. One branch of this field of study deals with the anisotropy of magnetic susceptibility (AMS) as a strain history indicator. AMS data for any sample may be expressed as a triaxial ellipsoid whose major, intermediate and minor axes represent the relative susceptibility magnitudes and azimuths. The total ellipsoid shape and orientation reflects the overall directional fabric of the sample, as expressed by magnetic mineral grains (Khan 1962). Application of the method to volcanic rocks relies on the assumption that the petrofabric expressed by magnetic grains bears a simple relationship to the strain history. Empirically, this assumption appears to be justified; for example, there is generally a close correspondence between the visible macroscopic petrofabric expressed by fiamme in welded tuffs with their AMS ellipsoids. The most useful application of AMS in volcanology appears to be as an indicator of flow direction; previous studies have attempted to determine movement directions of magma in dykes (Ellwood 1978; Knight and Walker 1988), and of primary particulate pyroclastic flows which produce welded tuffs (Ellwood 1982; Knight 1985; Knight et al. 1986). The latter are problematic; given the influence that phenocryst textures, depositional mechanisms, groundmass crystallisation, compaction, welding and rheomorphism could all have on the final mean orientation of magnetic grains within the tuff, it is perhaps surprising that apparently meaningful flow directions can be extracted from ignimbrites using AMS. In this paper, we speculate on the origin of AMS fabrics observed in tuffs and demonstrate in one case that the heterogeneous character of welded tuffs composed of fiamme, lithics and matrix has not seriously affected AMS fabrics. We then apply the method to the interpretation of the deformational and flo-

Offprint requests to: JA Wolff

wage history of a welded-tuff dyke from the mid-Tertiary Trans-Pecos Texas igneous province.

Measurement of AMS

Measurement of AMS may employ a number of different types of induction instruments; very sensitive balanced coils or bridges, cryogenic magnetometers, torsion fibre magnetometers, and spinner magnetometers. Methods have been reported by a number of authors including King and Rees (1962) and Stone (1963) for torsion fibre instruments; Noltimier (1967) for spinner magnetometers; and Scriba and Heller (1978) and Schmidt et al. (1988) for cryogenic magnetometers. In the spinner and torsion fibre method (which we employ), elements of the AMS ellipsoid are measured using the spinner or torsion fibre magnetometer but the initial susceptibility is measured independently. Investigators using the AMS method generally measure rock samples in the form of drilled cores ~2.5 cm in diameter which have been sliced into lengths of ~2.2 cm to conform to an optimum length to diameter ratio range of 0.82–0.90 (Banerjee and Stacey 1967; Noltimier 1971).

AMS data for any rock specimen are conventionally expressed as triaxial ellipsoids whose major, intermediate and minor axes represent the corresponding maximum (χ_1), intermediate (χ_2) and minimum (χ_3) susceptibility magnitudes and azimuths (magnitude ellipsoid of Nye 1969). Mass susceptibility is calculated from these magnitudes and given as:

$$\chi = (\chi_1 + \chi_2 + \chi_3)/3 \quad (1)$$

Previous AMS studies of welded tuffs

Ellwood (1982) studied the AMS characteristics of the densely welded Fish Canyon, Wason Park, Carpenter Ridge and Masonic Park ignimbrites of the central San Juan Mountains, Colorado. He found, in general, a pronounced subhorizontal magnetic foliation, defined by the plane containing the maximum and intermediate AMS ellipsoid axes. This would be expected to result from compaction and welding under vertical uniaxial stress imposed by gravity. However, at most sampled sites, maximum and intermediate axes were respectively clustered rather than randomly dispersed about the horizontal, such that the maximum axis projected towards the known source for each tuff unit. In other words, the long axis of the AMS ellipse was found to parallel plausible primary flow directions in each ignimbrite. Ellwood commented that this linear fabric, imposed upon the dominant planar fabric, is characteristic of megascopic petrofabrics in rheomorphic welded tuffs. He also noted localized severe disturbance of magnetic fabric by rheomorphism within the Fish Canyon Tuff.

In rheomorphic flow, the welded tuff body behaves as a coherent viscous fluid, and the magnetic fabric develops as a function of grain alignment in response to flow, much as it does in a lava or dyke (Ellwood 1978, 1979; Knight and Walker 1988). Inasmuch as rheomorphic flow is slope-controlled and therefore generally tends to duplicate primary flow directions, rheomorphic tuffs might be expected to yield plausible 'primary' flow direction estimates. However, the possibility remains that a component of the lineation really is inherited from the primary particulate flow. If so, it must in some way be related to an ignimbrite depositional mechanism which causes grain alignment in the final rock body to duplicate the direction of movement of the primary pyroclastic flow. If primary lineation can be preserved, it should be detectable in tuffs that are not sufficiently densely welded to have undergone rheomorphism.

Knight et al. (1986) carried out a comprehensive AMS study of the Toba Tuffs of Sumatra, and used their results to determine flow directions and infer source vents. Significantly, they found a well-developed magnetic fabric, with good separation of long and intermediate AMS ellipsoid axes, in partly welded tuff samples that appear not to have suffered rheomorphism. Knight et al. (1986) argue that, in order for magnetic fabric to reflect flow alignment, the fabric must be carried by non-equant ferrimagnetic mineral grains that were present as particles in the primary pyroclastic flow, and were deposited with their long axes aligned in the direction of flow.

Although not explicitly stated by Knight et al. (1986), the most likely carriers of magnetic fabric in this interpretation are titanomagnetite phenocrysts liberated into the pyroclastic matrix during explosive disruption of magma. Although such grains will certainly contribute to any fabric, their role as major contributors may be questioned on two grounds: (1) titanomagnetite is an isotropic mineral that typically crystallises with an octahedral habit (this is especially true of phenocrysts), and is not prone to forming elongate grains; (2) it is present as phenocrysts in only minor or trace amounts in the Fe-poor felsic magmas that erupt to form ignimbrites.

It is important to note here that it is not necessary for the magnetic grains to be non-equant and aligned in order to impart a detectable AMS to a sample. The effect may also arise through organisation of equant grains into planar or linear arrangements. As a schematic example, consider a single layer of steel ball bearings on a flat surface. Each individual ball is spherical and therefore isotropic. However, the whole layer defines a planar fabric and possesses a pronounced planar AMS.

Ellwood and Howard (1981) provided an experimental demonstration, with direct geologic relevance, of this effect. They used sand-sized quartz grains coated either with fine (0.25 μm) maghemite or magnetite powders in some experiments, and coarse (125 μm) magnetite powder in others, to study particle orientations in an experimentally produced barchan dune. Their AMS results from the coated-quartz experiments mirrored the flow behavior of non-coated quartz and loose, coarse magnetite grains. Therefore the AMS signature was produced by arrangement of very fine grains around much larger particles, where only the large particles are directly affected by depositional processes. Analogous to this effect is crystallisation of magnetic minerals within a pre-existing directional fabric, as seen in high oxygen fugacity olivine basalts where very fine, exsolved magnetite is observed to coat large olivine phenocrysts. In welded tuffs, submicroscopic iron oxide grains commonly grow within the eutaxitic texture around flattened shards and in squashed vesicles in fiamme. It is not necessary that the grains actually be growing during the strain episode that is responsible for the fabric (although this may impart some shape anisotropy to grains and therefore enhance the effect), but merely that the grains be arranged along fabric elements.

This provides a link between the primary flow directions of pyroclastic flows and the AMS characteristics of the final rock. Several studies (Elston and Smith 1970; Froggatt et al. 1981; Suzuki and Ui 1982, 1983; Kamata and Mimura 1983) have shown that non-equant particles and objects carried by pyroclastic flows frequently assume a preferred alignment parallel to the flow direction. This arises from alignment of particles during bulk laminar flow or deposition within a basal shear layer to a plug flow, although very large objects such as the tree logs described by Froggatt et al. (1981) may yield flow directions for turbulently emplaced units such as the Taupo ignimbrite. These depositional fabrics result from the response of rigid objects to their enclosing flowing medium, and should not be confused with so-called primary laminar viscous flow features in very densely welded tuffs (Schmincke and Swanson 1967; Chapin and Lowell 1979), which arise from the deformation of hot, soft clasts during deposition. The majority of particles within pyroclastic flow deposits (pumice fragments, glass shards, crystals of common silicate minerals, and any lithics from a well-jointed rock) are markedly non-equant, and are likely to exhibit a degree of preferred alignment if flow and depositional conditions are favourable. This alignment will have a linear component parallel to flow direction. In the absence of post-welding rheomorphism, this linear element should be capable of surviving welding, which is the consequence of vertically directed uniaxial stress and produces a purely planar fabric (if the tuff is not resting on a steep slope). Growth of fine-grained iron oxides within the welded tuff fabric then results in an AMS fabric with both prolate (inherited from the primary flow) and oblate (largely the product of welding) character. The overall AMS ellipsoid is oriented with long and intermediate axes defining the plane of welding, while the long axis parallels the flow azimuth. This AMS signature is ubiquitous in published studies of welded tuffs. We suggest that, although dispersed magnetite phenocrysts within a welded ignimbrite matrix will affect the shape of the AMS ellipsoid, that disseminated groundmass magnetic grains make the dominant contribution. Some recent work by Schlinger et al. (1988) supports our argument: these authors describe the dominant role played by groundmass Fe-oxide microlites as magnetic remanence carriers in volcanic glass, and note the significance of magnetic-mineral microlites in the interpretation of AMS fabrics from welded tuffs.

Intra-sample AMS variations in a welded tuff

No previous study has attempted to determine the effect of the various welded tuff components (pumice, lithics, matrix) on intra-sample AMS precision. Intra-sample variations might also shed light on the relative contributions of phenocrysts and groundmass iron oxides to the magnetic fabric. Therefore, a single large (0.5 m) sample of densely welded ignimbrite, chosen because of its abundant large (several cm) fiamme and lithics, and strong visible eutaxitic texture, was studied in some detail.

The sample was taken from flow unit 5 of the Battleship Rock Tuff at the type locality in San Diego Canyon, Jemez Mountains, New Mexico (Bailey et al. 1969; Self et al. 1988). It consists of black, vitrophyric fiamme set in a grey matrix of welded shards, lithics and crystals. In thin section, the matrix has a grey-brown colour imparted by sub-micron sized opaque microlites that are preferentially concentrated around the margins of flattened shards, and within flattened vesicles in fiamme. The arrangement of microlites thus follows the dominant welding fabric, although within the limits of resolution of the petrographic microscope (0.5 μm), individual microlites show no preferential alignment. In the field, there was no apparent directional fabric within the welding foliation plane, such as might result from primary flow alignment or subsequent rheomorphism.

In the laboratory three orthogonal slabs (labelled *X, Y, Z*) were cut from the sample with the *Z* slab parallel to foliation. Each slab was then polished, and fiamme shape and orientation measured using a binocular microscope and an arbitrary zero initial azimuth. Fiamme deforming around lithics were excluded. The data were used to estimate the strain ellipse for each surface using the method of Dunnet (1969) for deformation of initially randomly oriented ellipses; results are listed in Table 1. Despite the rather large inherent errors, the average of 4.25 of the strain ratios deduced for the *X* and *Y* slabs respectively is consistent with complete porosity loss of pumices with initially 76% vesicles, in excellent agreement with a range of 78%–80% vesicles calculated from density measurements on pumices taken from non-welded lateral equivalents of Battleship Rock flow units (S. Self, personal communication). This demonstrates that the fiamme have suffered only pure porosity-loss flattening, without rheomorphism. Results for the *Z* slab confirm that there is no preferred orientation of pumice fragments in the plane of flattening, either due to rheomorphism or primary flow alignment. The close agreement between the deduced average initial shape ratio (Ri) for *X* and *Y* slab pumices, and the measured mean (Rf) of *Z* slab pumices (Table 1), tends to confirm this.

Standard specimens for AMS analysis were then drilled from each slab (*Z* slab = 10 specimens; *X* slab = 13 specimens; *Y* slab = 7 specimens). Care was taken to incorporate some large lithic fragments and fiamme in five cores respectively and five cores were also carefully recovered from matrix zones where large fiamme and lithic fragments could be avoided.

Table 1. Results of strain analysis of fiamme in the Battleship Rock sample

	X slab	*Y* slab	*Z* slab
Rs	4.0	4.5	—
Ri	1.6	1.6	—
Rf (mean)	4.5	5.3	1.6
N	74	69	35

Strain analysis by the method of Dunnet (1969). *Rs, Ri* deduced strain ellipse and initial mean axial ratio of clasts respectively assuming initial random orientations; *Rf* measured axial ratios; *N* number of measurements. Note that *Ri* values for the *X* and *Y* slabs are equal to the measured *Rf* value for the *Z* slab, which was cut parallel to foliation (see text)

AMS laboratory procedures

AMS was measured for all specimens using low-field torsion fibre magnetometers and a susceptibility bridge. The magnetic fabric parameters reported in Table 2 for the Battleship Rock were calculated from these measurements and conform to parameters suggested for AMS data by Ellwood et al. (1988). These include magnetic foliation (*f*) where:

$$f=(\chi_2/\chi_3)/\chi \text{ (Khan 1962)} \quad (2)$$

and lineation:

$$l=(\chi_1/\chi_2)/\chi \text{ (Khan 1962)} \quad (3)$$

Table 2. Mean susceptibility data for Battleship Rock (BS-) and Castellan dyke (C-) sample sets

Site	*N*	$\chi \times 10^{-4}$	*V*	*l*	*f*
BS-*X*	13	66.2	68.7	1.004	1.022
BS-*Y*	7	67.2	65.7	1.006	1.028
BS-*Z*	10	62.5	65.6	1.004	1.020
BS-PF	5	68.7	68.0	1.005	1.029
BS-*F*	5	66.5	65.3	1.006	1.030
BS-*L*	5	65.6	65.2	1.005	1.021
C2-1-1	6	0.6	43.7	1.003	1.002
C2-2-1	8	1.8	53.5	1.009	1.016
C2-3-1	8	1.7	45.7	1.013	1.014
C2-4-1	6	2.4	60.6	1.007	1.019
C2-5-1	4	2.5	71.0	1.003	1.018
C2-6-1	6	1.7	67.4	1.004	1.027
C2-10-1	8	1.2	45.9	1.008	1.007
C2-11-1	4	1.5	55.7	1.008	1.017
C3	8	1.7	45.7	1.013	1.014
C4	8	1.5	62.6	1.005	1.017

Total $N=99$

N number of samples; χ, mean susceptibility in SI units relative to a mass of 1 g (Eq. 1); *V* Graham's parameter *V* (Eq. 4); *l* magnetic lineation (Eq. 3); *f* magnetic foliation (Eq. 2)

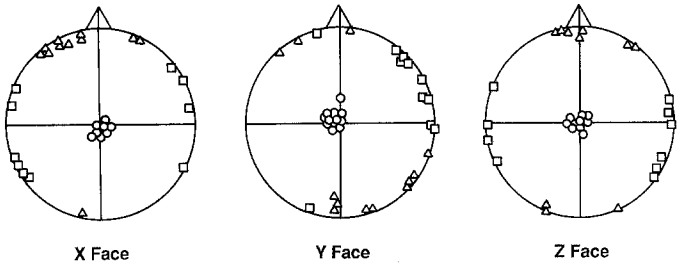

Fig. 1. AMS principal axis equal area plots for the *X*, *Y* and *Z* slabs cut from the Battleship Rock sample. Arbitrary plot orientation. These and all subsequent plots are upper hemisphere, equal area where *squares* = maximum, *triangles* = intermediate, and *circles* = minimum principal axes of the AMS ellipsoid

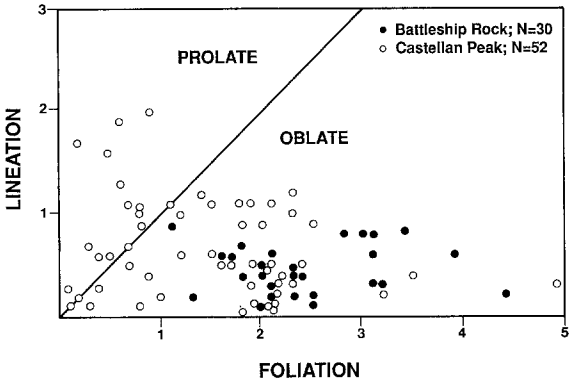

Fig. 2. Foliation-lineation AMS diagram for all samples, where $f=(\chi_2-\chi_3)/\chi$ and $l=(\chi_1-\chi_3)/\chi$

Both are indicators of the general character of the fabric.

For characterising the AMS ellipsoid shape we use Graham's (1966) parameter *V*, where:

$$\sin^2 V=(\chi_1-\chi_2)/(\chi_2-\chi_3) \quad (4)$$

The ellipsoid is oblate if $V>45°$; prolate if $V<45°$.

Results

AMS results for the Battleship Rock sample are shown in Figs. 1-3 and Tables 2 and 3. Bulk susceptibility ranges between $6\text{-}7\times10^{-3}$ in SI units relative to 1 gm mass. AMS distribution data indicate tight minimum axial clusters with poor (but significant) long and intermediate axial clusters (Fig. 1), consistent with the dominant oblate fabric pattern imposed by welding (Fig. 2).

Measurement of the alignment of elements in the Battleship Tuff sample indicates a close correspondence between the petrofabric and magnetic fabric orientations. It is clear that AMS axial consistency is excellent, even when large lithic fragments are included in individual samples (Fig. 3). Also, directions measured optically for Battleship Rock slabs show a close correspondence with AMS orientations, even though the petrofabric data are constrained to measurement in a single plane while the AMS data represent 3-dimensional orientations of magnetic fabric elements. Table 3 gives the orientation data for optical measurement of elongated elements (small fiamme) in the *X*, *Y*, and *Z* slabs cut from the Battleship Rock block. These are contrasted with the AMS data and the agreements are striking. For example, the angle α, representing the mean angular difference between measured lineated elements and the horizontal plane in slabs *X* and *Y* and *Y*-lithics, compares closely to the angle β representing the AMS linear elements in the horizontal plane ($\beta=90-\chi_3$ azimuth). Examination of the Battleship Rock block indicates a well-defined foliation which is clearly identified in the AMS

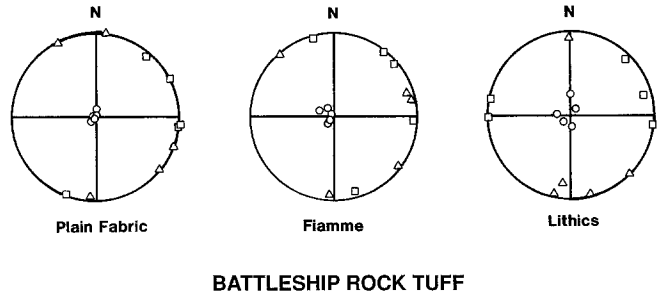

Fig. 3. AMS principal axis plots of Battleship Rock samples drilled from slabs, grouped according to the dominant component in the sample. *Plain fabric* denotes matrix-dominated samples with a minimum fiamme and lithic content. Arbitrary plot orientation

Table 3. Comparison of optical and AMS orientation data for Battleship Rock Tuff

	Optical			AMS	
	N	$\overline{Rf}$	α	*N*	β
X	74	4.5	5.4°	10	4.9°
Y	69	5.3	3.7°	13	4.7°
Z	35	1.6	—	10	2.7°
y-Lithoclasts	8	1.4	4.5°	5	3.5°

Rf, N as Table 1: α, optically measured departure of eutaxitic texture from the horizontal; β, AMS data ($90-\chi_3$ inclination), representing departure of magnetic foliation from the horizontal. α and β are measured relative to the same arbitrary initial horizontal

data, best illustrated in Table 2 and Figs. 1-3. All three slabs exhibit a persistent slight elongation. The resolution and treatment of the optical strain measurements are insufficient to show this. This separation of long and intermediate AMS axes within the dominant plane of foliation may be either the expression of a fabric reflecting preferential alignment of fragments prior to welding, or of slight rheomorphism following welding. In either case, AMS appears to be a more sensitive indicator of petrofabric than quantitative optical study.

Very little difference is observed between Battleship Tuff samples dominated by large lithic fragments, large flattened fiamme, and matrix (Fig. 3; Table 2). Clearly, the various components have not significantly disrupted the magnetic fabric distributions; while some scatter is evident, the gross character of the data are similar. Therefore it is expected that unobserved anomalous fabric elements (lithics, fiamme) contained within paleomagnetic samples may contribute to the scatter in the data, but not significantly alter the result. It is interesting to note that thin-section examination of large Battleship Rock fiamme suggests that the scatter in AMS data for fiamme-rich samples can be attributed to the variable alignment of magnetite phenocrysts within pumice clasts, which it is assumed, were initially randomly oriented.

Application to a welded-tuff dyke

Geological setting

A discontinuous series of small dykes of trachytic welded tuff occurs on a small rocky hill 1 km northwest of Cerro Castellan, Big Bend National Park, in the Tertiary Trans-Pecos Texas volcanic province. The tuff is emplaced into heavily zeolitised Oligocene basalts of the Bee Mountain Member of the Chisos Formation; the exact age of the intrusion is unknown. It contains lithics of an underlying Cretaceous limestone unit. Eutaxitic texture is well-preserved at the margins, however, for much of its thickness the dyke has been welded to a dense, homogeneous vitrophyre in which fiamme cannot easily be discerned. Where seen, the fiamme frequently define an imbricated fabric with respect to dyke walls. Although patchily altered, the generally good state of preservation of the tuff, with abundant glass, demonstrates that it substantially post-dates the hydrothermally altered basalts. The tuff-dyke is typically less than 1 m wide, and is restricted to the margins of a large (ca. 150 m diameter) block of country-rock rotated some 70° with respect to the regional tilt. The occurrence is interpreted as an explosive vent that became plugged when this block slid or fell into the conduit, although whether this occurred during or immediately after the explosive activity is unclear from field relations.

Field and laboratory procedures

Nine oriented hand samples, collected from dyke exposures at the north, south and east sides of the rotated block, were returned to the laboratory where individual specimens were drilled from each sample. At the principal exposure, three individual samples (C2-2; C2-3; and C2-4), including both cooling margins (maximum dyke width = 40 cm) were recovered at 10 m increasing height intervals along the same dyke segment. Here the rotated block forms the NW wall of the dyke, while in situ country rock forms the SE wall; the dyke itself dips steeply to the SE. Closely spaced core specimens were drilled from each of these samples. The lowermost sample (C2-2) was recovered from a section of the dyke which exhibited obvious columnar jointing between the cooling margins. This sample was further sampled by cutting slabs (C-3; C-4) each 3 cm thick from the sample with surfaces oriented normal to the long axis of the column. Since columnar segment C2-2 was oriented at a slight angle to the cooling margins of the dyke, these slab surfaces were oriented sub-parallel with the dyke margins. Six cores from C-3 and eight cores from C-4 were drilled for AMS measurement.

Remanent moment (RM) measurement after alternating field (AF) induction to 30 mT was also performed on specimens cut from samples C2-2,

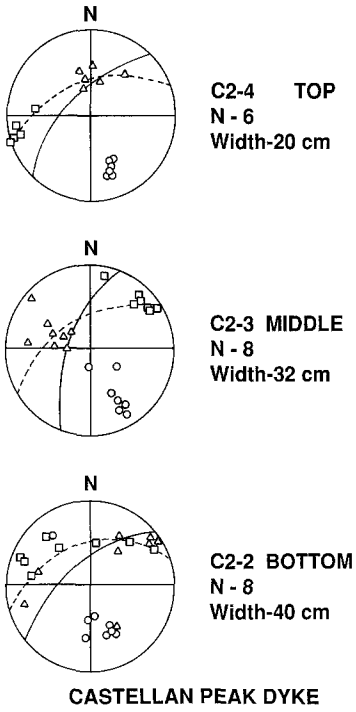

Fig. 4. AMS principal axis plots for Castellan dyke samples. *N*, magnetic North at the site; *solid great circle,* orientation of the dyke in the field; *dashed great circle,* magnetic foliation plane defined by χ_1 and χ_2 orientations

C2-3, and C2-4 using a Molspin Minispin spinner magnetometer. Density determinations were performed on specimens from C2-3 and C2-4.

Results

The dominant AMS fabric distribution for this suite of samples is oblate in character ($V > 45°$; Table 2) with some samples exhibiting a neutral to prolate character (Fig. 2, Table 2). Susceptibility in dyke samples is significantly less than in Battleship Rock samples (Table 2). In general, all the AMS distribution data indicate poor to moderate long and intermediate axial clusters but good to excellent minimum axial clusters (Figs. 4 and 5). These data are consistent with the dominant oblate fabric patterns (Fig. 2).

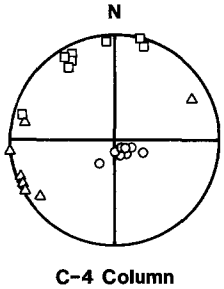

Fig. 5. AMS principal azimuth equal area, upper hemisphere plot for one of the columnar cross sections (C-4) cut from Castellan dyke segment C2-2. Arbitrary plot orientation

Table 4. RM data for Castellan dyke

Site	*N*	*D*	*I*	$M \times 10^{-2}$	*K*	α_{95}
C2-1-1	5	161.1	−60.8	4.2	154.0	6.2
C2-2-1	8 (7)	139.8	−59.0	5.4	391.6	3.1
C2-3-1	8	133.9	−50.0	7.8	376.8	2.9
C2-4-1	6	158.9	−58.7	4.2	963.4	2.2
C2-5-1	4 (3)	144.8	−55.9	1.5	635.9	4.9
C2-6-1	6	140.6	−58.5	5.0	407.0	3.3
C2-10-1	8	135.3	−55.0	7.2	517.7	2.4
C2-11-1	4	145.1	−51.4	6.1	81.9	10.2
C2-W1-1	4	138.2	−67.4	7.6	243.3	5.9
C2-W2-1	4	131.0	−66.0	6.1	127.0	8.2
Mean		142.9	−58.6	5.5	113.5	4.6

Castellan $\Theta' = 58°$ $\phi' = 194.8$ $\delta_p = 8.8$ $\delta_m = 9.0$
Irving & Irving (1982) at 30 Ma $\Theta' = 86°$ $\phi' = 154°$
Tilt ~30° along a N20E azimuth
D, *I*, mean RM declination and inclination; *M*, mean total moment in Am^2; *K* and α_{95} are statistical estimates of precision from Fisher (1953). High *K* and low α_{95} indicate good precision. Θ' and ϕ' are paleopole latitude and longitude, respectively. δ_p and δ_m are standard estimates of precision for the calculated poles

The RM directions exhibit excellent within site and between site precision but a paleopole (Table 4) calculated for these Tertiary samples does not conform to other stable North American poles of equivalent age (e.g. the 30 Ma pole of Irving and Irving (1982); Table 4) nor does it represent a recent main field overprint. Rotating our pole to correspond with that of Irving and Irving (1982) suggests the Castellan area has been tectonically tilted down ~30° along an azimuth of N20° E. This result is consistent with the regional tilt in the area. If such tilting has occurred, the dyke segment represented by these samples was originally sub-vertical. The consistency in the data suggests that no differential rotation has occurred between individual dyke segments.

Density variations across the dyke at the principal sampling locality are axially symmetric (Fig. 6), with the densest material in the dyke centre. RM exhibits similar increases in the central portion of dyke segments, while susceptibility is generally inversely correlated with density and RM (Fig. 7). AMS axial distributions for these same samples show several interesting variations. The χ_3 axes are generally well clustered, the mean

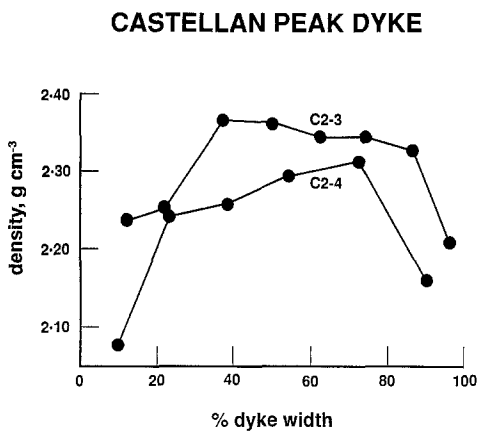

Fig. 6. Density profiles across Castellan dyke segments C2-3 and C2-4

is relatively consistent from bottom to top of the dyke segment (Fig. 4) and all the axial clusters show improvement from the bottom to the top of the dyke. The χ_1 and χ_2 axial distributions define a great circle (magnetic foliation plane) which varies at an angle of 10°–40° to the orientation of the dyke in the field at the point of sampling. The intermediate axis lies in the plane of the dyke, and the long axis direction coincides with the maximum angular separation between fabric plane and dyke plane. The fabric is thus consistently imbricated throughout the dyke thickness. Visible imbrication of fiamme is apparent where the tuff is not completely welded to a homogeneous black vitrophyre, mostly at the margins.

Stresses produced by thermal contraction are affecting some observed AMS distributions. Thermal stresses are the primary cause of columnar jointing in many igneous rock types (e.g. Spry 1962). Columnar jointing is variably developed in the main dyke segment. Sample C2-2 was a single column; two 4 cm segments were cut from this sample, subsampled, and the data reported in Fig. 5 and Table 2 (samples C3 and C4). The data in Fig. 5 represent typical data for columns developed in dykes (Ellwood 1979), where the magnetic foliation plane is oriented normal to the axis of the column, the result of principal uniaxial stresses building up along the axis of the column due to thermal contraction. In some dyke segments such thermal stresses may be the dominant control on AMS fabric; however, the imbricated fabric, which is oblique to dyke walls and columns, was not produced in this way.

The chilled, less densely welded margins which define the welding profile through the dyke (Fig. 6) possess distinct magnetic characteristics, including low magnetic moments at the margins which increase, as does density, toward the dyke center (Fig. 7). Susceptibility exhibits inverse values which are interpreted to reflect decreasing magnetic grain sizes or decreasing magnetic grain concentrations toward the center of the dyke. Thin section examination indicates that the dyke matrix has a higher concentration of opaque mineral microlites than do fiamme, in part because the microlites appear to form in response to reaction between silicate magma and limestone lithics. The absence of large fiamme at the margin may be responsible for the higher bulk susceptibility. Alternatively, the more porous nature of the less-densely welded margins may have allowed locally higher oxygen fugacities to develop during microlite formation, aiding the crystallisation of magnetic minerals.

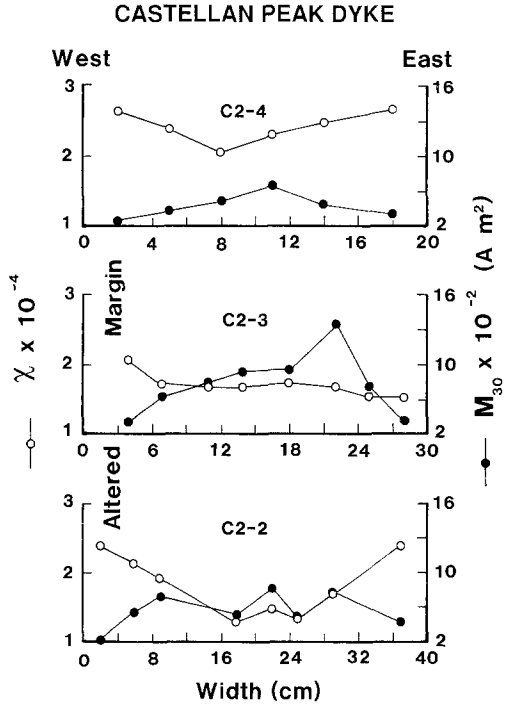

Fig. 7. Susceptibility *(open symbol)* and remanent moment *(closed symbol)* profiles across three Castellan dyke samples at the principal exposure, from lowermost C2-2 to topmost C2-4. Susceptibility (χ) relative to 1 gm mass samples (SI) and remanent moment in (M_{30}) Am^2 after 30 mT demagnetisation

Discussion

Intrusive welded tuffs in which the welding fabric is parallel to subvertical intrusive contacts are

widely distributed volcanic rock forms. They are generally thought to represent quenched feeders or vents for explosive eruptions and present an intriguing contrast to surface tuffs in that gravitational load pressure has clearly not played the major role in compaction and welding. Two mechanisms have been proposed. Almond (1971) and Wolff (1986) suggested that closure of the conduit choked with hot pyroclastic material at the end of an explosive eruption, perhaps in response to waning magmatic pressure, exerted a horizontally directed uniaxial stress on the contents to produce a subvertical eutaxitic texture. Upward rheomorphism of the welded mass is a conceivable mechanism for the appearance of a lava dome composed of degassed magma over the vent site at the end of an explosive eruption (Wolff 1986). In contrast, Reedman et al. (1987) proposed that the Weolseong welded tuff plug in Korea resulted from laminar shearing of soft clasts in a boundary layer during deposition of the tuff by agglutination along the walls of an active vent feeding an explosive eruption. Reedman et al.'s mechanism is essentially the same as that of primary laminar viscous flowage or 'primary welding' proposed for surface flows by Schmincke and Swanson (1967) and Chapin and Lowell (1979).

Fabric studies should be able to distinguish between these two mechanisms. Boundary-layer shearing and agglutination should impart a pronounced prolate character to the agglutinated material, which Reedman et al. (1987) have documented for the Weolseong plug. However, the same fabric could be produced by rheomorphism in Wolff's model. More crucial evidence in support of the essentially agglutinated character of the Weolseong plug provided by Reedman et al. is the systematic inward variation in lithic content and lithology, indicating layer-by-layer accretion, and the inward *decrease* in the intensity of welding, the opposite of which would be expected from horizontal compaction.

The application of AMS to this problem lies in its ability to detect matrix fabrics that are not readily apparent to the eye. A weak prolate element subparallel to the intrusive contact in welded-tuff matrix taken from dyke samples which do not display macroscopic evidence for rheomorphism (including down-vent rheomorphic creep) would tend to support the primary depositional model; it is difficult to see how this could be pervasively developed in pyroclastic material choking a vent after the termination of an explosive eruption. Rheomorphism as in Wolff's (1986) mechanism should result in highly variable prolate fabric development as the welded tuff is squeezed between rough-surfaced dyke walls.

Dyke formation

The axially symmetric density profiles (Fig. 6) and systematic variations in bulk magnetic properties attributable to grain size (Fig. 7) across the Castellan dyke are consistent with the conduit closure and welding mechanism envisaged by Almond (1971) and Wolff (1986), with the most densely welded tuff formed in the center of the unit. However, the persistently lineated and imbricated character of the oblate AMS fabric is more consistent with the boundary layer shearing and agglutination model of Reedman et al. (1987). It is significant that the fabric is consistently imbricated throughout the dyke thickness, and that (assuming generally upward flow) the sense of imbrication indicates deposition of clasts against the side of the rotated block. Upward rheomorphism of dyke contents should result in (if any) imbrication against both margins of the dyke. The less densely welded margins of the dyke also exhibit the imbricated fabric. Occasionally, the marginal 1 cm of the dyke is finer grained than the interior and lacks the largest fiamme, reminiscent of the fine-grained basal layer commonly seen in pyroclastic flow units (layer 2a of Sparks et al. 1973); this suggests that, prior to deposition and welding, the pyroclastic mass moved past this surface as some form of grain flow.

Our preferred explanation of the data is that the dyke is the remnant of an explosive vent which was plugged, and the eruption shut off, when wall failure occurred and a large block of country rock slid or rotated into the vent. As the block entered the vent, hot pyroclastic material became plastered against it to form a layer of agglutinated tuff with imbricated fiamme; the imbrication formed either by shearing of hot, soft clasts within the boundary layer of the eruption mixture passing the block surface, or by direct agglutination of fragments onto an inclined surface. Final compression and welding occurred as the block settled into place, squeezing the accumulated layer of agglutinated material against the vent wall. Chilling against block and wall retarded welding at the margins, after the manner of a conventional welded tuff. Thus the effects of both 'primary welding' (i.e. deformation of clasts during deposition) and welding *sensu stricto* can be detected in the dyke.

'Primary welding' in conduits

Identification of depositional and welding mechanisms in very densely welded, rheomorphic, lava-like ignimbrites emplaced on the surface has generated debate for some time (Schmincke and Swanson 1967; Chapin and Lowell 1979; Wolff and Wright 1981; Eckren et al. 1984; Trigila and Walker 1986; Henry et al. 1988; Henry et al. in press). Syn-depositional deformation of clasts (often termed 'primary welding') is much more likely to occur in a volcanic conduit than in a pyroclastic flow travelling over the Earth's surface, because of the high velocities and temperatures of an eruption mixture that has not yet been ejected into the atmosphere. It may occur in two ways: by shearing of clasts in the bulk flow or by agglutination of individual clasts onto an adjacent static surface. The first mechanism can only operate if the clasts have a similar viscosity to the shearing matrix, which is unlikely to be the case for any moving flow except at the point the bulk flow is sufficiently dense for matrix particles to interact and adhere, i.e. during deposition. However, the second mechanism would be favoured in relatively dilute flows, where large clasts can impact directly onto an adjacent surface. Where observed, the texture of the dyke described in this paper generally resembles that of a pyroclastic flow deposit, in that the bulk material would have been matrix-supported prior to compaction. This suggests that the first mechanism may have been dominant in this case: compression of the erupting mixture to the point where matrix particles began to adhere may have occurred in response to entry of the block which ultimately plugged the conduit.

Deposition of an erupting mixture onto conduit walls by either mechanism may be more common than is generally recognised, and may occur without the rather special conditions deduced here. Progressive accumulation of soft clasts on the walls of the Weolseong welded tuff intrusion described by Reedman et al. (1987) apparently took place as the eruption proceeded, not as it ended through conduit blockage.

Other evidence for syn-eruptive agglutination within conduit-vent systems during explosive eruptions is provided by the common occurrence of aggregate pumices in pyroclastic deposits. An aggregate pumice is a pumice clast with an internal structure of variably deformed smaller pumices set in a lithic-bearing and, typically, fines-depleted matrix. The structure is usually clast-supported with point-contact welding providing coherence; internal bedding is absent. The density of an aggregate pumice is usually low; they are not re-erupted fragments of welded tuff as described, for example, by Wright (1981). Aggregate pumices appear to form irrespective of magma composition; they have been found (field observations by the first author) in the pantelleritic Oira and 6.3 ka Tuhua tephras (Mayor Island, New Zealand), in the phonolitic Granadilla Pumice (Tenerife, Canary Islands), and in the high-silica rhyolite Upper Bandelier Tuff (Jemez Mountains, New Mexico). There is no apparent control of eruptive style on their formation: the Oira tephra forms a small, locally dispersed strombolian pumice cone (Houghton et al. 1985), the Tuhua and Granadilla are plinian/ignimbrite deposits in the 1–10 km^3 range of erupted magma volume, while the Upper Bandelier is a major continental silicic ignimbrite of some 250 km^3. There is no systematic relation between grain-size distributions within aggregate pumices and their host pyroclastic units; clast- and matrix-supported aggregate pumices may be found in both fall deposits and ignimbrites. We regard them therefore as having formed from direct deposition of the primary erupting mixture onto the walls of the conduit-vent system, rather than as re-erupted fall-back material. Their low density implies rapid re-disruption and incorporation back into the erupting mixture.

Conclusions

1) AMS fabrics in welded tuffs are mainly controlled by groundmass magnetic minerals, the distribution of which reflects existing fabric elements within a tuff sample. An AMS fabric results from the combined effects of primary flow lineation (if any), welding and rheomorphism (if any).
2) AMS is a more sensitive fabric indicator than quantitative optical studies, at least for densely welded tuffs.
3) Variable proportions of fiamme, lithics and matrix within a sample do not significantly affect AMS fabrics in densely welded tuffs.
4) The welded-tuff dyke exposed near Cerro Castellan, Trans-Pecos Texas, formed through both 'primary welding' and laterally directed squeezing between walls, in response to wall failure and vent closure by a large block of country-rock.
5) Lining of conduit walls by adhering hot, soft pyroclastic material may be a more common process in explosive eruptions than hitherto realised.

Acknowledgements. We are grateful to the U.S. Dept. of the Interior National Park Service, Southwest Region for permission to collect samples within Big Bend National Park, to Reggie Overman for assistance in the field, and to Steve Self for drawing our attention to the Castellan dyke and for general discussion. Tony Reedman suggested several improvements to our first draft. Funding for BBE was provided from SARR research funds.

References

Almond DC (1971) Ignimbrite vents in the Sabaloka cauldron, Sudan. Geol Mag 108:159–176

Bailey RA, Smith RL, Ross CS (1969) Stratigraphic nomenclature of volcanic rocks in the Jemez Mountains, New Mexico. US Geol Surv Bull 1274:1–19

Banerjee SK, Stacey FD (1967) The high field torque-meter method of measuring magnetic anisotropy in rocks. In: Collinson DW, Creer KM, Runcorn SK (eds) Methods in paleomagnetism. Elsevier, Amsterdam, pp 470–476

Chapin CE, Lowell FR (1979) Primary and secondary flow structures in ashflow tuffs of the Gribbles Run paleovalley, central Colorado, in Ash Flow Tuffs, edited by CE Chapin and WE Elston. Spec Pap Geol Soc Am 180:137–154

Dunnet D (1969) A technique of finite strain analysis using elliptical particles. Tectonophysics 7:117–136

Eckren EB, McIntyre DH, Bennett EH (1984) High-temperature, large-volume, lavalike ash-flow tuffs without calderas in southwestern Idaho. US Geol Surv Prof Paper 1272:1–76

Ellwood BB (1978) Flow and emplacement direction determined for selected basaltic bodies using magnetic susceptibility anisotropy measurements. Earth Planet Sci Lett 41:254–264

Ellwood BB (1979) Anisotropy of magnetic susceptibility variations in Icelandic columnar basalts. Earth Planet Sci Lett 42:209–212

Ellwood BB (1982) Estimates of flow direction for calc-alkaline welded tuffs and paleomagnetic data reliability from anisotropy of magnetic susceptibility measurements: central San Juan Mountains, southwest Colorado. Earth Planet Sci Lett 59:303–314

Ellwood BB, Howard JH III (1981) Magnetic fabric development in an experimentally produced barchan dune. J Sediment Petrol 51:97–100

Ellwood BB, Hrouda F, Wagner J-J (1988) Symposia on magnetic fabrics: Introductory comments. Phys Earth Planet Inter 51:249–252

Elston WE, Smith EI (1970) Determination of flow direction of rhyolitic ash flow-tuff from fluidal textures. Geol Soc Am Bull 81:3393–3406

Fisher RA (1953) Dispersion on a sphere. Proc R Soc London Ser A 217:295–305

Froggatt PC, Wilson CJN, Walker GPL (1981) Orientation of logs in the Taupo Ignimbrite as indicator of flow direction and vent position. Geology 9:109–111

Graham JW (1966) Significance of magnetic anisotropy in Appalachian sedimentary rocks. In The earth beneath the continents, JA Steinhert and TJ Smith eds. Am Geophys U Washington D.C. 627–648

Henry CD, Price JG, Rubin JN, Parker DF, Wolff JA, Self S, Franklin R, Barker DS (1988) Widespread, lavalike silicic volcanic rocks of Trans-Pecos Texas. Geology 16:509–512

Henry CD, Price JG, Parker DF, Wolff JA (in press) Mid-Tertiary silicic alkalic magmatism of Trans-Pecos Texas: rheomorphic tuffs and extensive silicic lavas. Tour guide 9A, IAVCEI general Assembly, Santa Fe, 1989

Houghton BF, Wilson CJN, Weaver SD (1985) Strombolian deposits at Mayor Island: "basaltic" eruption styles displayed by a peralkaline rhyolitic volcano. New Zealand Geol Surv Record 8:42–51

Irving E, Irving GA (1982) Apparent polar wander paths Carboniferous through Cenozoic and the assembly of Gondwana. Geophys Surv 5:141–188

Kamata H, Mimura K (1983) Flow directions inferred from imbrication in the Handa pyroclastic flow deposit in Japan. Bull Volcanol 46:277–282

Khan MA (1962) Anisotropy of magnetic susceptibility of some igneous and metamorphic rocks. J Geophys Res 67:2873–2885

King RF, Rees AI (1962) The measurement of the anisotropy of magnetic susceptibility of rocks by the torque method. J Geophys Res 67:1565–1572

Knight MD (1985) Stratigraphy and anisotropy of magnetic susceptibility of the Toba ignimbrites, North Sumatra. MS thesis, Univ Hawaii at Manoa pp 279

Knight MD, Walker GPL (1988) Magma flow directions in dikes of the Koolau complex, Oahu, determined from magnetic fabric studies. J Geophys Res 93:4301–4319

Knight MD, Walker GPL, Ellwood BB, Diehl JF (1986) Stratigraphy, paleomagnetism and magnetic fabric of the Toba tuffs: constraints on the source and eruptive styles. J Geophys Res 91:10355–10382

Noltimier HC (1967) The use of the spinner magnetometer for anisotropy measurements. In: Collinson DW, Creer KM, Runcorn SK (eds) Methods in paleomagnetism. Elsevier, Amsterdam, pp 399–402

Noltimier HC (1971) A model for grain dispersion and magnetic anisotropy in sedimentary rocks. J Geophys Res 76:3990–4002

Nye JR (1969) Physical properties of crystals. Oxford Univ Press, New York, pp 322

Reedman AF, Park KH, Merriman RJ, Kim SE (1987) Welded tuff infilling a volcanic vent at Weolseong, Republic of Korea. Bull Volcanol 49:541–546

Schlinger CM, Rosenbaum JG, Veblen DR (1988) Fe-oxide microcrystals in welded tuff from southern Nevada: origin of remanence carriers by precipitation in volcanic glass. Geology 16:556–559

Schmidt VA, Ellwood BB, Nagata T, Noltimier HC (1988) The measurement of anisotropy of magnetic susceptibility (AMS) using a cryogenic (Squid) magnetometer and a comparison with results from a torsion-fiber magnetometer. Phys Earth Planet Inter 51:365–378

Schmincke H-U, Swanson DA (1967) Laminar viscous flowage structures in ash-flow tuffs from Gran Canaria, Canary Islands. J Geol 75:641–664

Scriba H, Heller F (1978) Measurements of anisotropy of magnetic susceptibility using inductive magnetometers. J Geophys 4:341–352

Self S, Kircher DE, Wolff JA (1988) The El Cajete Series, Valles Caldera, New Mexico. J Geophys Res 93:6113–6127

Sparks RSJ, Self S, Walker GPL (1973) Products of ignimbrite eruptions. Geology 1:115–118

Spry A (1962) The origin of columnar jointing, particularly in basalt flows. Geol Soc Aust J 8:191–216

Stone CB (1963) Anisotropy of magnetic susceptibility measurements on a phonolite and on a folded metamorphic rock. Geophys J 7:375–390

Suzuki K, Ui T (1982) Grain orientation and depositional ramps as flow direction indicators of large-scale pyroclastic flow deposits, Japan. Geology 10:429–432

Suzuki K, Ui T (1983) Factors governing the flow lineation of a large-scale pyroclastic flow — an example in the Ata pyroclastic flow deposit, Japan. Bull Volcanol 46:71–81

Trigila R, Walker GPL (1986) The Onano spatter flow, Italy: evidence for a new ignimbrite depositional mechanism. Int Volc Cong New Zealand 1986 Abstr:81

Wolff JA (1986) Welded-tuff dykes, conduit closure, and lava dome growth at the end of explosive eruptions. J Volcanol Geotherm Res 28:279–284

Wolff JA, Wright JV (1981) Rheomorphism of welded tuffs. J Volcanol Geotherm Res 10:13–34

Wright JV (1981) The Rio Caliente Ignimbrite: analysis of a compound intraplinian ignimbrite from a major late Quaternary eruption. Bull Volcanol 44:189–212

Received July 28, 1988/Accepted October 18, 1988